Journal of ELECTRONIC MATERIALS, Vol. 49, No. 1, 2020
https://doi.org/10.1007/s11664-019-07767-6

Removal of Lead by Tetra Hydroxyl Phenyl Porphyrin-Linked Magnetic Nanoparticles: Process Optimization by Using Taguchi Design Method

ENSIEH GHOLAMREZAPOR [1] and ABBAS ESLAMI [1,2,3]

1.—Department of Inorganic Chemistry, Faculty of Chemistry, University of Mazandaran, P.O. Box 47416-95447, Babolsar, Iran. 2.—e-mail: eslami@umz.ac.ir. 3.—e-mail: eslami_a@yahoo.co.uk

Fe_3O_4@SiO_2@THPP (MSTHPP) nanocomposite was prepared as an adsorbent for the removal of lead ions. The structural characteristics of this nanocomposite were determined using Fourier transform-infrared (FT-IR) spectroscopy, scanning electron microscopy (SEM), transmission electron microscopy, x-ray diffraction, vibrating sample magnetometry (VSM), and N_2 adsorption-desorption analyses. SEM images showed that the magnetic nanoparticles have uniform morphologies with a mean size of 20 nm. The magnetic properties of the synthesized nanocomposite were measured on a VSM with maximum saturation magnetization values of 40 $emug^{-1}$ and 10 $emug^{-1}$ for Fe_3O_4@SiO_2 and MSTHPP nanocomposites, respectively. MSTHPP has been efficiently used to remove lead ions from aqueous solutions. After the lead sorption process, the nanocomposite was magnetically separated from the mixture and showed good reusability. The effects of pH, contact time, adsorbent dosage and initial concentration of lead in the removal of lead were investigated. Optimization of the parameters was performed by using Taguchi design method to obtain the maximum removal efficiency. The optimized condition can be achieved when pH, contact time, adsorbent dosage and initial concentration of lead are 5.3 min, 30 min, 50 mg, 20 ppm, respectively. The M, MS, and MSTHPP lead removal efficiency was found to be 18%, 25%, and 97%, respectively.

Key words: Porphyrin, magnetic particles, Taguchi method, lead removal

INTRODUCTION

The heavy metal, lead, is highly toxic to many organisms and, therefore, is considered a polluting threat for the environment and water resources.[1,2] The broad industrial applications of lead, which ranges from fabrication of electronic devices and batteries to dye industries, raises a serious concern about the possibility of leakage into the environment.[3,4] Lead uptake may result in several serious health problems for humans such as blood enzyme changes, hyperactivity and neurological disorders.[5,6] Therefore, the removal of lead ions from wastewater is very crucial for public health. Heavy metal ions can be removed from wastewater using several methods such as ion exchange,[7] chemical precipitation,[8] reverse osmosis, membrane filtration,[9] electrolysis and adsorption,[10] out of which the latter is usually preferred as it is cheaper and more effective for wastewater purification and widely used in clean-up processes.[11] Different adsorbents, such as zeolites, activated carbon, clays, minerals, resins, metal oxides, and bio-adsorbents have been investigated for the removal of heavy metal ions.[12] Although adsorption methods are suitable for removal of heavy metal ions from aqueous solutions, they suffer from two main limitations: low adsorption capacity and difficult

(Received May 9, 2019; accepted October 24, 2019; published online November 12, 2019)

separation of the adsorbent from water. In recent years, nanoscience and nanotechnology have been used for the resolution of such environmental problems.[13] Nanometer sized materials have attracted significant interest due to their special properties such as high specific surface area, which make them excellent potential adsorbents for various species such as heavy metal ions.[14,15] However, due to the small size of nanoparticles, their physical separation may be somewhat difficult, but this problem can be overcome through attachment of adsorbents to the magnetic nanoparticles and employment of a strong external magnetic field to separate magnetic nanoparticles from solution.[16–18] In several recent investigations, this approach has been exploited for removal of various species including arsenate, phosphate and heavy metals.[19–22] The Fe_3O_4(magnetite) is the most studied magnetic nanoparticle for the aforementioned application due to its unique properties such as high specific surface area and superparamagnetic characteristic which means it can be attracted to a magnetic field, but residual magnetism is not preserved after removing the field.[23,24] However, this magnetic feature causes aggregation of magnetite nanoparticles which is undesirable for practical purposes. To prevent the aggregation, the magnetite nanoparticles must be coated with a suitable coating agent such as surfactants, small organic molecules, polymers, and metal oxides such as SiO_2.[25–27] The protecting shells can be used for stabilization of the magnetic nanoparticles and also for functionalization.[28–30] The porphyrin derivatives play key roles in various science fields. They act as chelating ligands for most metals and can tightly bind to soft heavy metals and, therefore, may be used as adsorbents.[31] Porphyrins and an SiO_2 shell can usually be linked through different functional groups present on the porphyrins such as carboxylic acid, sulphonic acid, salicylate, acetylacetonate, and hydroxyl derivatives.[32–34] In the present study, tetra hydroxyl phenyl porphyrin (THPP, Scheme 1) has been immobilized on Fe_3O_4@SiO_2 (MS) and used as an adsorbent for removal of lead ions. Porphyrin can be strongly linked to the silica layer with four hydroxyls.[35] To achieve maximum removal capacity of lead ions by the adsorbent, the experimental parameters can be optimized by means of statistical experimental design techniques.[36] The Taguchi method is known as a strong, high-quality experimental design method and can be exploited for optimization of the values of the experimental parameters through an effective and systematic approach. Many successful applications of Taguchi methods have been reported to improve several adsorption processes.[37–39] So, in this work, optimization of various parameters such as pH, contact time, absorber dosage and initial concentration of lead ion has been performed by Taguchi experimental design.

EXPERIMENTAL DETAILS

Ferric chloride hexahydrate ($FeCl_3{\cdot}6H_2O$), ferrous chloride tetrahydrate ($FeCl_2{\cdot}4H_2O$), NH_4OH, acetone, ethanol, polyvinylpyrrolidone (PVP), tetraethyl orthosilicate (TEOS), 4-hydroxybenzaldehyde, nitrobenzene, propionic acid, glacial acetic acid, and petroleum ether were all of analytical grade from Merck and Fluka chemical companies and used without further purification, except pyrrole, which was distilled before use. Deionized water was utilized in all experiments. FT-IR spectra were recorded with samples in KBr pellet and the range 4000–400 cm^{-1} on a FT-IR Bruker vector 22 spectrometer. UV–Vis spectra were recorded by a Baric 2100 model UV–Vis spectrophotometer. ^1H NMR, ^{13}C-NMR spectra were recorded at room temperature using a Bruker DRX 400 MHz–Avance III apparatus. The morphologies of the samples were characterized by scanning electron microscopy (SEM) using an LEO-1455VP microscope (acceleration voltage 10 kV) and transmission electron microscope (TEM, Zeiss - EM10C - 100 kV). The x-ray diffraction (XRD) measurement was performed with a Bruker D8 diffractometer using graphite monochromatic copper radiation (Cu Kα) at 40 kV,30 mA over the 2θ range 20–80°. The magnetic properties of the samples was measured using a vibrating sample magnetometer (VSM, MDK, and Model 7400) at room temperature. The textual properties of prepared compounds were analyzed by N_2 adsorption/desorption at liquid-nitrogen temperature (77 K) (INC-Belsorp II, Japan). Lead atomic absorption spectroscopy (AAS) was performed on an Atomic Absorption Spectrometer Varian Spectra AA 110.

Preparation of Fe_3O_4@SiO_2@THPP (MSTHPP)

The synthetic route for preparation MSTHPP, as indicated in Scheme 1, was carried out in four stages as follows: (a) magnetite nanoparticles, M, were prepared via co-precipitation.[40] A mixture of 8 g of $FeCl_3{\cdot}6H_2O$ and 2.9 g of $FeCl_2{\cdot}4H_2O$ dissolved in 80 ml deionized water was refluxed at 85°C under argon flow for 4 h. The pH of the solution was adjusted to 9 using NH_4OH (25% w/w) solution, and then the mixture was cooled to room temperature and the solids were washed by deionized water to pH 7. (b) A silica layer was coated onto the magnetite (M) via the sol–gel route. SiO_2-coated magnetite nanoparticles were prepared according to the previous procedures.[41–43] At first, 1 g PVP stabilized magnetite nanoparticles were dispersed in 200 ml ethanol. Then 6 ml NH_4OH (25% w/w) and 2 ml tetraethyl orthosilicate (TEOS) were added. This mixture was stirred for 24 h, a black precipitate was separated with an external magnetic field, and washed with ethanol several times. The product was dried in a vacuum oven. (c) Tetra hydroxyl phenyl porphyrin (THPP) was prepared according to the Rumyantseva method.[44] The

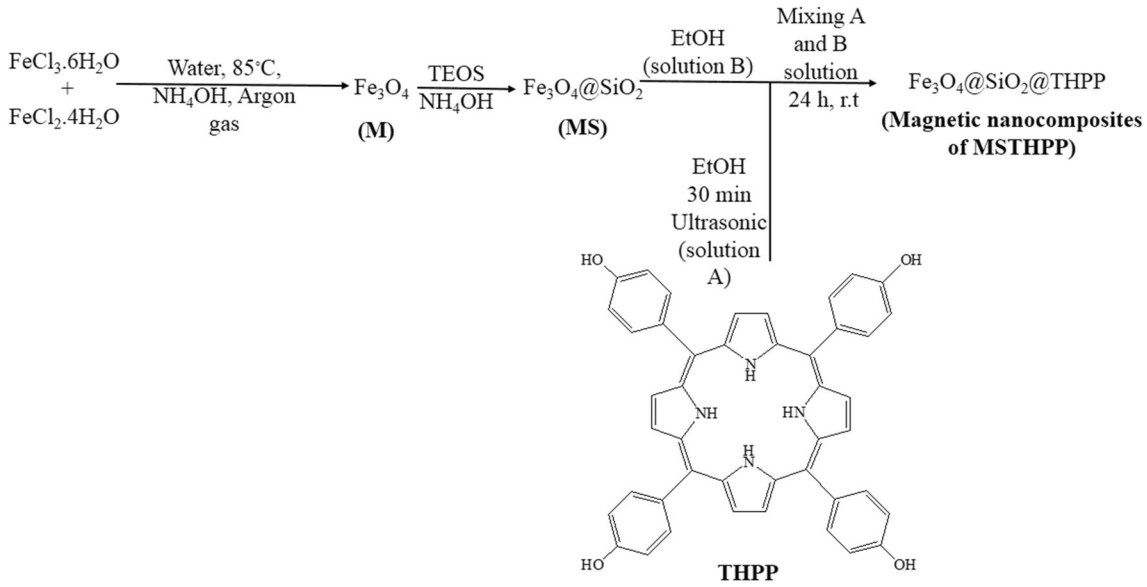

Scheme 1. Schematic model for the preparation of adsorbent.

products were characterized by FT-IR, UV–Vis, ^{1}H-NMR, and ^{13}C-NMR.

THPP: ^{1}HNMR (500 MHz, DMSO, ppm, TMS reference): 7.989–8.010 (m, 8H, orto-H), 7.198–7.219 (m, 8 meta-H), 8.866 (s, 8 pyrrole-H), 9.983 (s, 4 OH), −2.887 (br s, 2H, NH). ^{13}CNMR (400 MHz, $CDCl_3$ δ): 114.383 (meso-C), 157.790 (α-C), 120.738 (β-C), 132.237–136.070 (aromatic carbons). FT-IR (film on KBr, cm^{-1}): 3426 (O–H), 2366 (N–H), 2923 (C–H), 1605 (C aromatic), 1466 (C–N). UV–Vis (dichloromethane) λ *nm* (ε (M^{-1} cm^{-1})): 419 (3.2×10^5), 645 (3.1×10^2), 589 (1.2×10^2), 548 (1.1×10^2) and 514 (1.0×10^2)

(d) 0.08 *g* Fe_3O_4@SiO_2 (MS) nanoparticles were dispersed in 20 ml of absolute alcohol (Solution A). 0.04 g THPP was dispersed in 20 ml of absolute alcohol by ultrasonic irradiation for 30 min (solution B) and then was slowly step up to the solution A. This mixture was stirred at room temperature (24 h), then the solvent in the flask was evaporated and the solid was washed several times with deionized water.

Sorption Procedure

Lead adsorption by M, MS, and MSTHPP (as adsorbent) has been studied in different experimental conditions. A different amount of adsorbent was mixed with 10 ml of 20 ppm aqueous lead(II) nitrate solution, then adsorbent separated from other solution with using of an external magnetic field. The aqueous phase was magnetically decanted and lead concentration was calculated according to Eq. 1:

$$\text{Lead removal}\% = \frac{C_0 - C_i}{C_0} \times 100\% \qquad (1)$$

where C_0 and C_i are the initial and final concentrations of lead ions before and after the adsorption, respectively. The above process was schematically illustrated in Scheme 2.

Experiments Design

In order to optimize experimental parameters in removal of lead, a Taguchi-based experiment design was used. Standard L25 orthogonal array (four parameters and five levels) was used. The parameters, their levels and the standard L25 orthogonal array are shown in Table I and II. Minitab 17 software was employed for the calculation of optimization and analysis of the results of the control parameters.

RESULTS AND DISCUSSION

Characterization

The IR spectra of the M (Fe_3O_4), MS (Fe_3O_4@-SiO_2), MSTHPP nanostructures and THPP were shown in Fig. 1. In these spectra the bands at 1640 cm^{-1} and 3440 cm^{-1} can, respectively, be assigned to the O-H stretching and bending vibration modes of hydroxyl groups and the adsorbed water. For M (Fig. 1a), the bands at 577 cm^{-1} and 460 cm^{-1} can be attributed to the Fe-O stretching mode at the tetrahedral and octahedral sites, respectively. The spectrum of MS (Fig. 1b) shows characteristic peaks at 1050 cm^{-1} and 950 cm^{-1} corresponds to the asymmetric stretching of Si-O-Si bonds, and the bending vibration of the Si-O-H, respectively. These spectral results revealed the encapsulation of the Fe_3O_4 surface with the silica shell. Compared to pure MS, the MSTHPP nanocomposites show several other absorption bands at around 721 cm^{-1}, 795 cm^{-1} and 1600 cm^{-1}, which can be assigned to porphyrin skeletal vibrations. The other bands at 2850 cm^{-1},

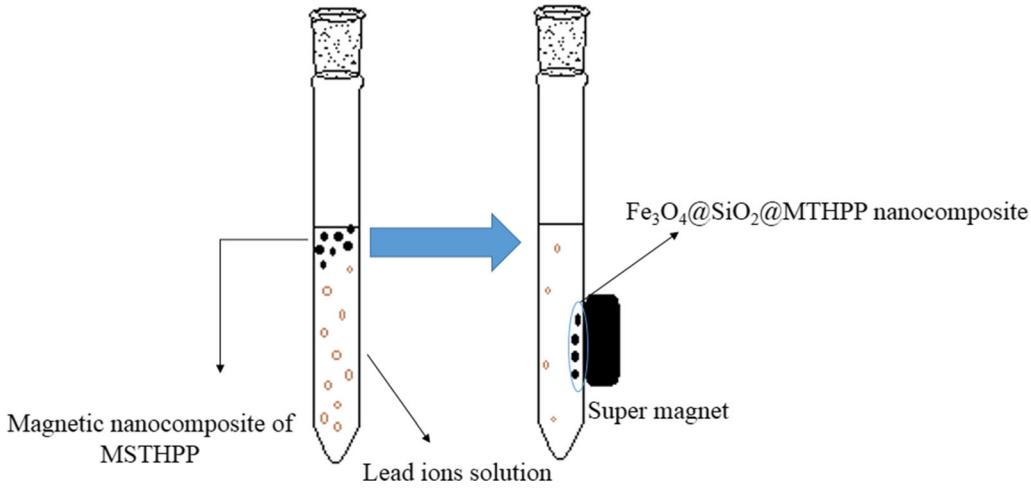

Scheme 2. Schematic representation of removal of lead ions from solution with magnetic adsorbent.

Table I. The selected parameters and their levels in Taguchi based experimental design

Parameters	Symbol	Level 1	Level 2	Level 3	Level 4	Level 5
pH	pH	3	4	5.3	7	9
Time contact (min)	Time	10	15	20	25	30
Initial Pb concentration (ppm)	Con	10	15	20	25	30
Amonut of adsorbent (g) × 100	Absorber	1	2	3	4	5

Table II. Taguchi L-25 orthogonal array design and Pb removal percent

Run	pH	Time contact (min)	Initial Pb concentration (ppm)	Amount of adsorbent (g) × 100	Pb removal (%)
1	3	10	10	1	10
2	3	15	15	2	15
3	3	20	20	3	20
4	3	25	25	4	25
5	3	30	30	5	20
6	4	10	15	3	25
7	4	15	20	4	30
8	4	20	25	5	33
9	4	25	30	1	10
10	4	30	10	2	25
11	5.3	10	20	5	66
12	5.3	15	25	1	35
13	5.3	20	30	2	25
14	5.3	25	10	3	97.3
15	5.3	30	15	4	96
16	7	10	25	2	20
17	7	15	30	3	25
18	7	20	10	4	60
19	7	25	15	5	70
20	7	30	20	1	45
21	9	10	30	4	80
22	9	15	10	5	95
23	9	20	15	1	35
24	9	25	20	2	42
25	9	30	25	3	50

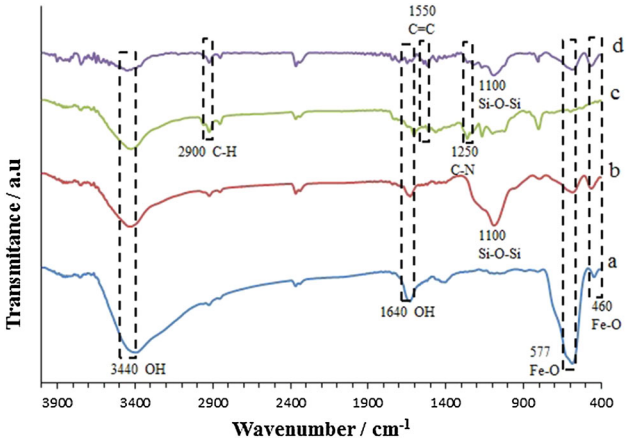

Fig. 1. FT-IR spectra of (a) M, (b) MS nanoparticles, (c) THPP, (d) MSTHPP nanocomposites.

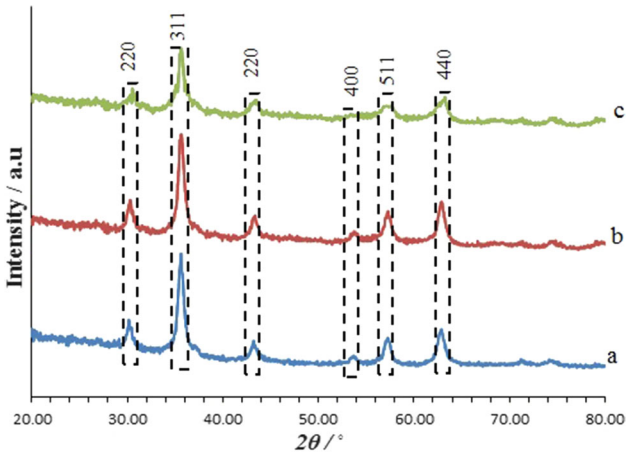

Fig. 2. XRD pattern of (a) M nanoparticles, (b) MS nanoparticles, (c) MSTHPP nanocomposites.

1640 cm^{-1}, 1550 cm^{-1} and 1250 cm^{-1} can be referred to C–H, O–H, C=C and C–N stretching vibrations of phenyl and pyrrole groups in THPP (Fig. 1c and d). The above results revealed that THPP was successfully coated on the surface of MS nanoparticles. The phase identity and crystalline structure of the nanocomposites were confirmed by XRD spectra and are shown in Fig. 2. The XRD pattern of M shows six characteristic diffraction peaks at 2θ = 30.2°, 35.5°, 43.2°, 53.6°, 57.1° and 62.7°, corresponding to (220), (311), (400), (422), (511) and (440) plans, respectively, that can be indexed to the pure cubic phase of Fe_3O_4 (JCPDS No.19-0629).[45] The average crystallite size of synthesized ferrite particles was estimated by Debye–Scherrer Eq. 2,[46] which was around 13.5 nm.

$$D = \frac{K\lambda}{\beta cos\theta} \quad (2)$$

where D is average crystallite size (nm), λ is the x-ray wavelength (nm), β is the angular width of the peak at full width half maximum height (FWHM)

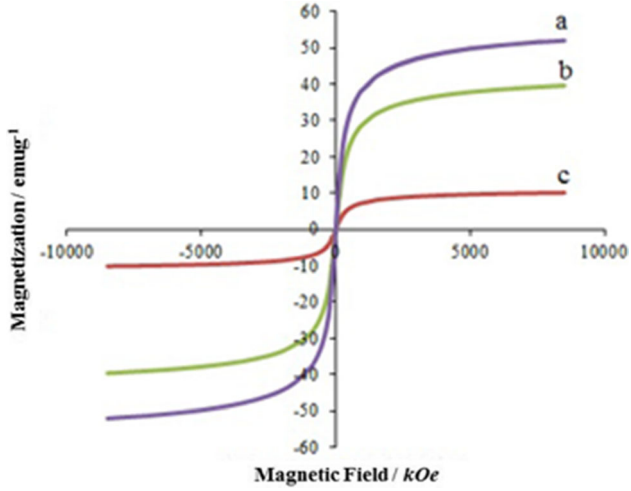

Fig. 3. Magnetization curves of (a) M nanoparticles, (b) MS nanoparticles, (c) MSTHPP nanocomposites.

(radians), K is a constant (K = 0.9), and θ is the characteristic diffraction angle (radians). The XRD pattern of MS shows the same diffraction peaks of the uncoated one (Fig. 2b) which confirms that the crystalline characteristic of the M is retained after the formation of the silica layer. The presence of silica as an amorphous phase was also confirmed by combining the results of FT-IR and XRD. Figure 2c illustrates the XRD pattern of the MSTHPP nanocomposite, in which the main characteristic peaks of the M retained after the coating of THPP on MS. In fact, the XRD result indicates that the THPP lie onto the surface of silica. The textural properties of the prepared particles were evaluated by N_2 adsorption–desorption isotherms. The investigated parameters are the Brunauer–Emmett–Teller (BET) surface area, BJH (Barrett, Joyner, and Halenda) pore volume and average pore widths which are 30.69 $m^2\ g^{-1}$, and 71.04 $m^2\ g^{-1}$, 0.034 $cm^3\ g^{-1}$, and 0.101 $cm^3\ g^{-1}$, 5.23 nm, and 6.04 nm for M and MS, respectively. The BET surface area, BJH pore volume, and average pore size of the MS particles were significantly increased with respect to M. The porous structures may facilitate metal absorption and increase the rate and extent of the removal reaction. The greater specific surface and pore volume of the nanocomposites can usually result in better removal efficiency. The magnetic properties of the M, MS and MSTHPP nanoparticles were measured using a vibrating sample magnetometer (VSM) at room temperature with a used field of $-$ 10 kOe $\leq$ H $\leq$ 10 kOe (Fig. 3). The measured magnetic saturation values of M, MS, and MSTHPP particles are 52 $emug^{-1}$, 39.6 $emug^{-1}$, and 10.10 $emug^{-1}$, respectively (Fig. 3a–c). The non-magnetic silica and THPP coating layers results in lower saturation magnetization of MS and MSTHPP particles with respect to that of M nanoparticles. However, the magnetization of MSTHPP (Fig. 3c) was still high

enough (10.10 $emug^{-1}$) to be magnetically separated by using an external magnetic field, which could ease the separation of nanocomposites from reaction solutions. The recovery of materials can be done by a water treatment process, and thus the recovery of materials is a key strategy that can reduce secondary pollution. In the absence of external magnetic field the nanocomposites can be well dispersed by shaking, indicated that the nanocomposites have good redispersibility and magnetic responsibility. The morphologies of the prepared nanoparticles were explored by by SEM images (Fig. 4). As seen in Fig. 4a, most of M nanoparticles were almost spherical in morphology with a diameter of 20–40 nm that is in good agreement with calculated value by the Debye–Scherrer equation. After silica coating, the MS particles have nearly a uniform diameter of 17–33 nm (Fig. 4b). As shown in Fig. 4c, MSTHPP particles has spherical shape with a diameter around 24-29 nm which is in good agreement with those calculated by the Debye–Scherrer equation. The TEM image (Fig. 4d) further confirms the results and revealed the core-shell structure of MSTHPP nanocomposites. The results were clearly supported the loading of THPP on the surface of the MS nanoparticles.

Adsorption Experiments

The contact time, pH, adsorbent dosage and initial concentration of lead are the main parameters of the experiments of adsorption of dissolved lead ions on the adsorbent MSTHPP and must be optimized. Since pH played a key role in the adsorption process and the adsorption of the lead onto the nano-adsorbent varies with pH, the performance of the adsorbent was studied in the relatively wide the pH range of 3.0–9.0 (20 mg/L Pb^{2+}, 50 mg adsorbent, room temperature, with contact time of 30 min) (Fig. 5a). The adsorption of lead ion initially increased with pH and reaches a maximum at pH = 5.3. Indeed, at lower pH the porphyrin central hole is partially protonated and unable to accept metal.[3] So, subsequent experiments were conducted at a pH of 5.3. The effect of contact time on removal efficiency was studied in the range of 10–40 min. The experiments were carried out in 20 mL of solution with pH of 5.3 (20 mg/L pb^{2+}, 50 mg adsorbent, contact time of

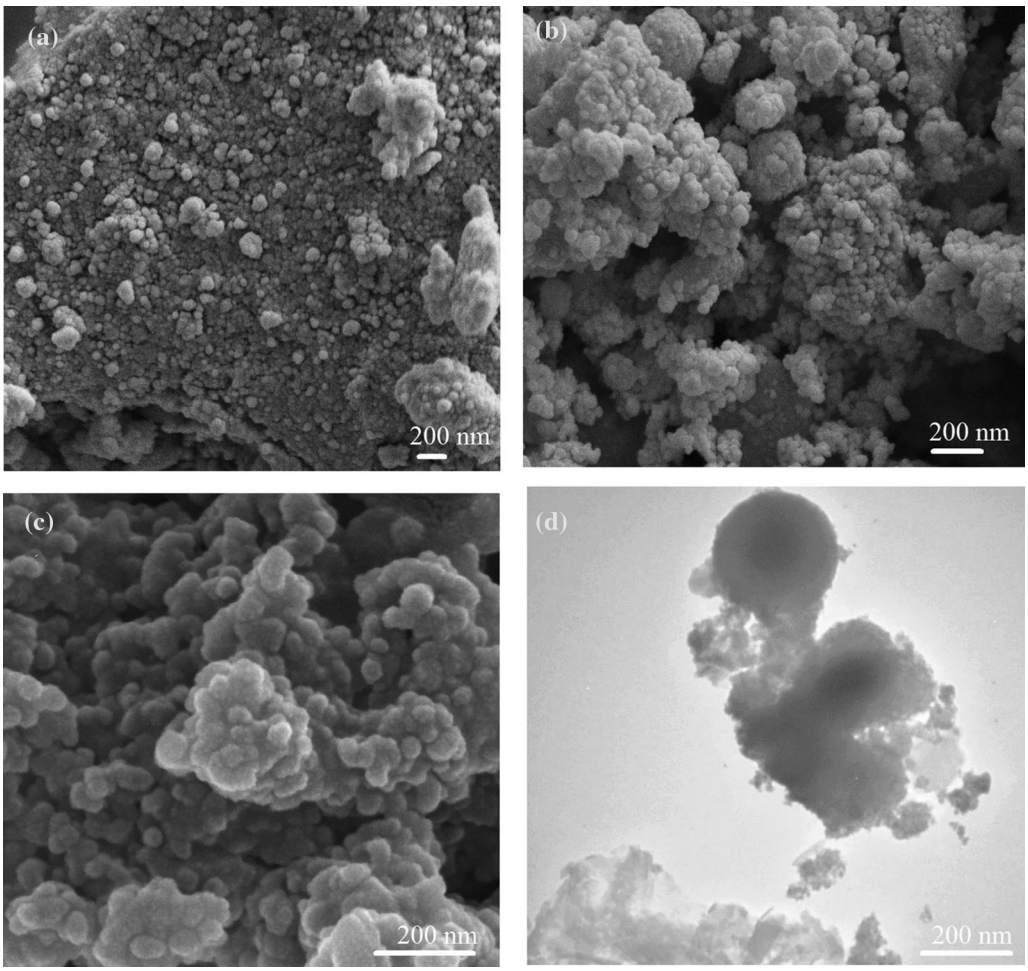

Fig. 4. SEM images of (a) M, (b) MS nanoparticles, (c) MSTHPP nanocomposites, (d) TEM image of MSTHPP nanocomposites,.

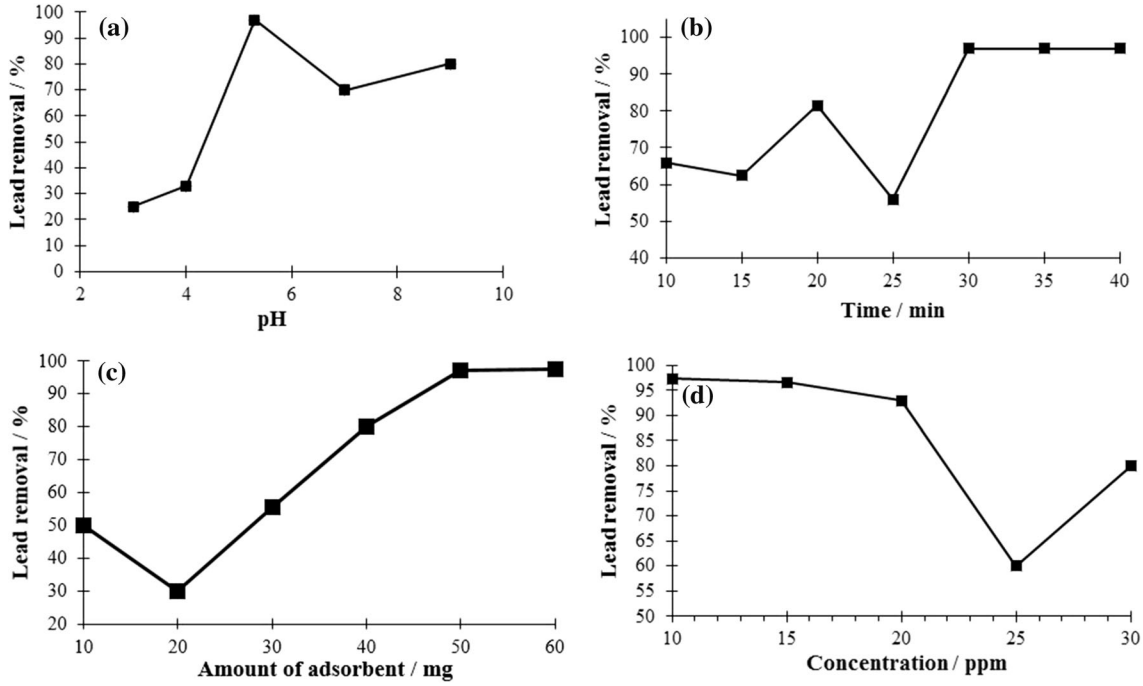

Fig. 5. Effect of (a) pH, (b) contact time, (c) adsorbent dosage, (d) initial lead ion concentration on the removal of lead ion in presence of the MSTHPP nanocomposite as a magnetic adsorbent.

30 min and room temperature). As shown in Fig. 5b the removal of lead ion from the solution increases with contact time and most of the lead ion was removed after 30 min and thereafter remained constant. Therefore, 30 min was considered as the optimum value for contact time in the subsequent experiments. The amount of adsorbent also plays a decisive role in improving removal efficiencies. So, the adsorption experiments were carried out using different amounts of absorbent from 10 mg to 60 mg for 20 mL of working solution (20 mg/L Pb^{2+}, contact time of 30 min, pH = 5.3, room temperature). As seen in Fig. 5c, an increase in dosage of the adsorbent increases the percent removal of lead ions and the maximum removal was obtained with 50 mg of adsorbent and then no further lead removal was observed by increasing the adsorbent dose. Therefore, 50 mg of the nanoadsorbents was selected as the optimum dose in the subsequent experiments. The effect of initial lead concentration on adsorption was also assessed by various the initial lead ion concentrations from 10 ppm to 30 ppm (30 min, 50 mg absorbent, pH = 5.3, room temperature). As it is illustrated in Fig. 5d, removal percent is constant from 10 ppm to 20 ppm, but it decreases upon further increase of initial lead concentration. Therefore, initial lead concentration of 20 ppm was selected for all the experiments. There are several active binding sites on the surface of adsorbent at low initial lead ion concentrations, and lead ions are easily removed. Since initial lead ion concentration becomes higher, the active binding sites are filled and saturated and little or no extra lead ions would be adsorbed, thus the removal

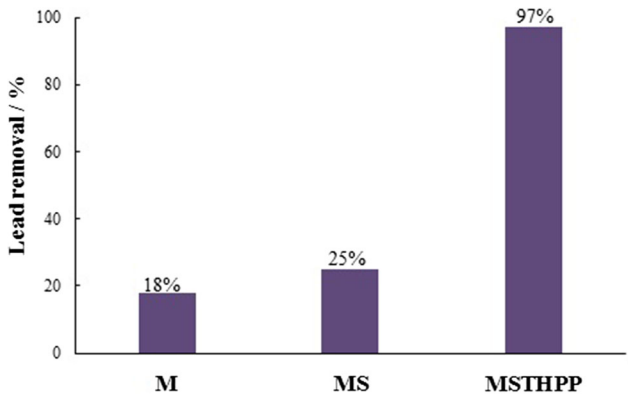

Fig. 6. The removal of lead ions in the presence of M, MS nanopartiles, and MSTHPP nanocomposite.

efficiency decreases. The removal of lead ions from water in presence of adsorbents of M, MS, and MSTHPP under optimum conditions has been demonstrated with the percent removal diagram in Fig. 6. The removal of lead ions from working solution in the presence of M, MS and MSTHPP adsorbent were found to be 18%, 25% and 97%, respectively. Three mechanisms were suggested to explain lead ion removal from aqueous solutions: (1) electrostatic adsorption, (2) complexation, and (3) ion exchange processes.[47] As mentioned above, the adsorption capacity of MSTHPP nanocomposite increases with increasing pH and reaches an optimum at the pH 5.3 (Fig. 5a). The result can be related to the fact that the complexation of porphyrin moiety in MSTHPP nanocomposite with lead ion is a pH-dependent process.[3,48] All the

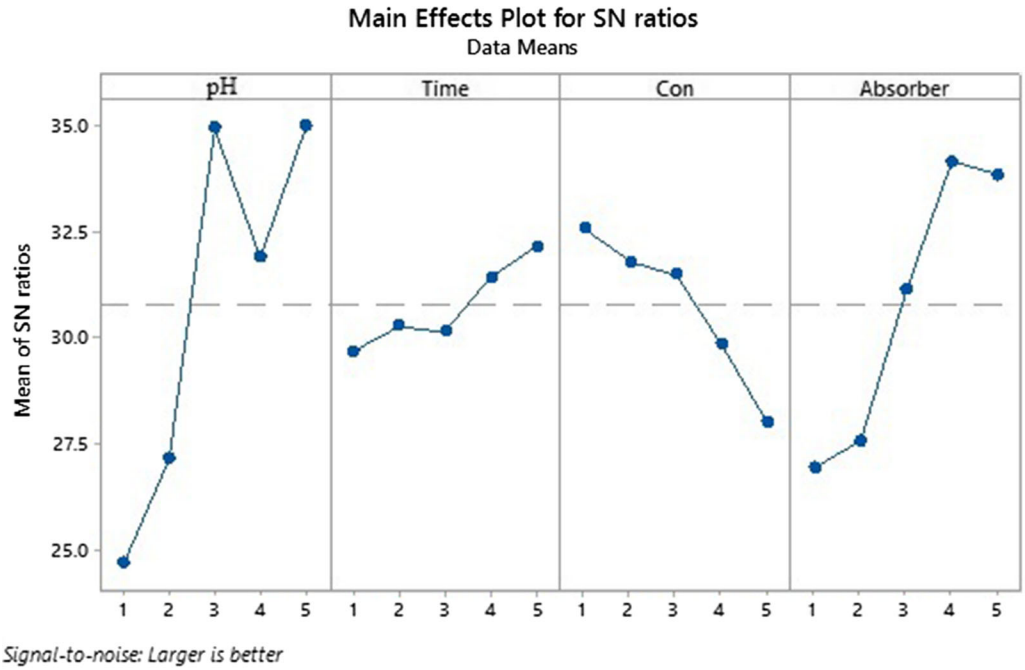

Fig. 7. Main effects plot of average *S/N* ratios of each parameter versus their values.

nanocomposites (M, MS, and MSTHPP) have surficial hydroxyl groups which may act as lead adsorbents, however, as shown in Fig. 6, the MSTHPP nanocomposite exhibits a distinguished lead removal potential with respect to M and MS. So, it can be concluded that the presence of a porphyrin ligand in the MSTHPP nanocomposite plays a key role in lead removal properties. Therefore, the dominant mechanism for the lead adsorption of the MSTHPP nanocomposite is presumably complexation of surficial porphyrin with lead ions.

Selection of Optimum Conditions Using Taguchi Design Method

The Taguchi design method was used to determine the optimum conditions and to select the parameters which have the strong impact on the removal of lead. The structure of Taguchi's orthogonal design and the results of percent removal of lead are shown in Table II and the highest value of lead percent removal (97.3%) was observed in the experiment No. 14. In the Taguchi method, the term 'signal' and 'noise' are the desirable and undesirable values for the output characteristic, respectively. The Taguchi method uses the signal-to-noise ratio (S/N ratio) to measure the amount of deviance from the desired value. Figure 7 shows the S/N ratios of the four parameters at five levels. It is clear that all the four parameters have the effects on the lead removal. The maximum value of the mean S/N value indicates the optimum value of the parameters. Figure 7 also indicates that the most important parameters in lead removal are pH and adsorbent value, because the difference between the maximum and minimum is great. The least important parameters were found to be time and lead concentration due to the small difference between the maximum and minimum. Therefore, the best combinations of the parameters for optimization of lead removal are 0.05 g adsorbent, 20 ppm initial concentration of lead, 30 min contact time, and pH 5.3, that is confirmed by plots of S/N values for all the four parameters. Among the four parameters, adsorbent and pH value have higher influence on lead removal.

CONCLUSION

Fe_3O_4@SiO_2@THPP (MSTHPP) nanocomposite was prepared through stepwise reactions and has been used for removal of lead from aqueous solution. The magnetic core was synthesized by co-precipitation method, and then a silica layer was coated onto the magnetite core via the sol–gel route, followed by surface modification of the silica layer with THPP. The experimental results revealed that the porphyrin molecules have been placed on the surface of the magnetite nanoparticle. The TEM image showed core-shell structure of the nanocomposite which is easily separable from solution by using an external magnetic field. The modification of the magnetic core with porphyrin results in a sharp increase in lead percent removal from 18% to 97%. Adsorption process was developed for lead removal by Taguchi optimization method. Taguchi evaluation of experimental data provides optimum amount of the parameters pH 5.3, contact time of 30 min, lead initial concentration of 20 ppm and adsorbent value of 0.05 g which increased lead percent

removal. The results of this study confirmed that the simultaneous Taguchi design method is considerably simpler than experimental methods. It was found that predicated optimum conditions of lead removal are well agreement with experimental results.

ACKNOWLEDGMENTS

We gratefully acknowledged financial support from the Research Council of the University of Mazandaran.

REFERENCES

1. M. Golshekan and S. Shariati, *Acta chem. Slov* 60, 358 (2013).
2. M. Emadi, E. Shams, and M.K. Amini, *J. Chem* 2013, 1 (2012).
3. T. Poursaberi, H. Ghanbarnejad, and V. Akbar, *J. Nano. Struct.* 2, 417 (2013).
4. E. Bilgin, M. Yuce, K. Kose, K. Erol, and D.A. Kose, *Hitite. J. Sci. Eng.* 4, 1 (2017).
5. S. Bakhshayesh and H. Dehghani, *Mater. Res. Bull.* 48, 2614 (2013).
6. E. Blicharska, M. Tatarczak-Michalewska, A. Plazińska, W. Plaziński, A. Kowalska, A. Madejska, M. Szymańska-Chargot, A. Sroka-Bartnicka, and J. Flieger, *J. Sep. Sci* 41, 3129 (2018).
7. H.M. Baker, A.M. Massadeh, and H.A. Younes, *Environ. Monit. Assess* 157, 319 (2009).
8. M.J. Gonzalez-Munoz, M.A. Rodriguez, S. Luque, and J.R. Alvarez, *Desalination* 200, 742 (2006).
9. M.G. Khedr, *Water Treat.* 2, 342 (2009).
10. Z.-H. Huang, X. Zheng, W. Lv, M. Wang, Q.-H. Yang, and F. Kang, *Langmuir* 27, 7558 (2011).
11. L. Fan, C. Luo, M. Sun, X. Li, and H. Qiu, *Colloid Surf. B. Biointerfaces* 103, 523 (2013).
12. X. Liu, Q. Hu, Z. Fang, X. Zhang, and B. Zhang, *Langmuir* 25, 3 (2008).
13. M. Khazaei, S. Nasseri, M.R. Ganjali, M. Khoobi, R. Nabizadeh, A.H. Mahvi, S. Nazmara, and E. Gholibegloo, *J. Environ. Health Sci. Eng.* 14, 1 (2016).
14. Y. Tan, M. Chen, and Y. Hao, *Chem. Eng. J.* 191, 104 (2012).
15. Z. Khayat Sarkar and F. Khayat Sarkar, *Int. J. Nanosci. Nanotechnol* 9, 109 (2013).
16. S. Rajput, C.U. Pittman Jr, and D. Mohan, *J. Colloid Interface Sci.* 468, 334 (2016).
17. A.Z.M. Badruddoza, Z.B.Z. Shawon, W.J.D. Tay, K. Hidajat, and M.S. Uddin, *Carbo. Poly* 91, 322 (2013).
18. X. Xin, Q. Wei, J. Yang, L. Yan, R. Feng, G. Chen, B. Du, and H. Li, *Chem. Eng. J.* 184, 132 (2012).
19. X. Peng, F. Xu, W. Zhang, J. Wang, C. Zeng, M. Niu, and E. Chmielewská, *Colloids Surf., A: Phys.Chem. Eng.Asp* 443, 27 (2014).
20. S. Recillas, A. Garcia, E. Gonzalez, E. Casals, V. Puntes, A. Sanchez, and X. Font, *Desalination* 277, 213 (2011).
21. M. Kumari, C.U. Pittman Jr, and D. Mohan, *J. Colloid Interface Sci.* 442, 120 (2015).
22. L. Dong, Z. Zhu, Y. Qiu, and J. Zhao, *Chem. Eng. J.* 165, 827 (2010).
23. P. Panneerselvam, N. Morad, and K.A. Tan, *J. Hazard. Mater.* 186, 160 (2011).
24. L. Sun, Y. Li, M. Sun, H. Wang, S. Xu, C. Zhang, and Q. Yang, *New J. Chem.* 35, 2697 (2011).
25. Y. Deng, D. Qi, C. Deng, X. Zhang, and D. Zhao, *J. ACS.* 130, 28 (2008).
26. R. Hao, R. Xing, Z. Xu, Y. Hou, S. Gao, and S. Sun, *Adv. Mater.* 22, 2729 (2010).
27. B.J. Kim, J. Bang, C.J. Hawker, J.J. Chiu, D.J. Pine, S.G. Jang, S.-M. Yang, and E.J. Kramer, *Langmuir* 23, 12693 (2007).
28. S. Hou, X. Li, H. Wang, M. Wang, Y. Zhang, Y. Chi, and Z. Zhao, *RSC Adv.* 7, 51993 (2017).
29. T. Sen, A. Sebastianelli, and I.J. Bruce, *J. ACS.* 128, 7130 (2006).
30. M.O. Ojemaye, O.O. Okoh, and A.I. Okoh, *J. Nanomater.* 2017, 1 (2017).
31. T. Poursaberi, V. Akbar, and S.M.R. Shoja, *Iran. J. Chem. Eng.* 34, 41 (2015).
32. E. Aguilera-Ruiz, U.M. García-Pérez, M. de la Garza-Galván, P. Zambrano-Robledo, B. Bermúdez-Reyes, and J. Peral, *Appl. Surf. Sci.* 328, 361 (2015).
33. J. Niu, B. Yao, Y. Chen, C. Peng, X. Yu, J. Zhang, and G. Bai, *Appl. Surf. Sci.* 271, 39 (2013).
34. W.M. Campbell, A.K. Burrell, D.L. Officer, and K.W. Jolley, *Coord. Chem. Rev.* 248, 1363 (2004).
35. E. Gholamrezapor and A. Eslami, *J. Mater. Sci: Mater. Elec.* 30, 4705 (2019).
36. V.N. Nair, B. Abraham, J. MacKay, G. Box, R.N. Kacker, T.J. Lorenzen, J.M. Lucas, R.H. Myers, G.G. Vining, and J.A. Nelder, *Technometrics* 34, 127 (1992).
37. P.T. Dhorabe, D.H. Lataye, A.R. Tenpe, and R.S. Ingole, *SN Appl. Sci.* 1, 250 (2019).
38. F. Googerdchian, A. Moheb, R. Emadi, and M. Asgari, *J. Hazard. Mater.* 349, 186 (2018).
39. V.C. Srivastava, I.D. Mall, and I.M. Mishra, *Chem. Eng. J.* 140, 136 (2008).
40. X. Zheng, L. Zhang, J. Li, S. Luo, and J.-P. Cheng, *Chem. Commun.* 47, 12325 (2011).
41. J.M. Perez, F.J. Simeone, Y. Saeki, L. Josephson, and R. Weissleder, *J. ACS.* 125, 10192 (2003).
42. M. Shokouhimehr, Y. Piao, J. Kim, Y. Jang, and T. Hyeon, *Angew. Chem.* 119, 7169 (2007).
43. A. Zielińska-Jurek, Z. Bielan, S. Dudziak, I. Wolak, Z. Sobczak, T. Klimczuk, and J. Hupka, *Catalysts* 7, 360 (2017).
44. V.D. Rumyantseva, A.S. Gorshkova, and A.F. Mironov, *Macroheterocycles* 6, 59 (2013).
45. N. Salamun, H.X. Ni, S. Triwahyono, A.A. Jalil, and A.H. Karim, *Malays. J. Fundam. Appl. Sci.* 7, 89 (2011).
46. A. Patterson, *Phys. Rev.* 56, 978 (1939).
47. Y. Liu, R. Fu, Y. Sun, X. Zhou, S.A. Baig, and X. Xu, *Appl. Surf. Sci.* 369, 267 (2016).
48. H. Ghanbarnejad, T. Poursaberi, and V. Akbar, *J. Nano. Struc.* 2, 417 (2012).